ISSN 1330–0008
CODEN FIZAE4

LASER-PRODUCED PLASMAS ON Mg, Al AND Si SURFACES

SANDA PLESLIĆ [a,1] and ŽELJKO ANDREIĆ [b]

[a] *Department of Applied Physics, Faculty of Electrical Engineering and Computing, University of Zagreb, Unska 3, 10000 Zagreb, Croatia*

[b] *Faculty of Mining, Geology and Petroleum Engineering, University in Zagreb, Pierottijeva 6, 10000 Zagreb, Croatia*

Dedicated to the memory of Professor Vladimir Šips

Received 29 October 2004; revised manuscript received 1 March 2005
Accepted 8 March 2005 Online 31 October 2005

Experimental investigations of laser-produced plasmas of Mg, Al and Si are described in this work. Plasmas were produced by nanosecond (6 ns) nitrogen-laser pulses ($\lambda = 337.1$ nm) with maximal energy density of about 1.1 J/cm^2 and were studied by UV-VIS spectroscopy. Electron densities of the order of 10^{18} cm^{-3} and electron temperatures of about 1.5 eV in the produced plasmas have been found. Numerical modelling of target heating gives 4 – 5 times higher electron temperatures than determined in experiments. Significant change of features of laser-produced plasmas on the three neighbouring elements has not been found. We show that optical depth of the materials is the main parameter for plasma production.

PACS numbers: 52.50.Jm UDC 533.9

Keywords: laser-produced plasma, Mg, Al and Si metal surfaces

1. Introduction

Plasma produced by laser radiation has been the subject of many investigations [1-7], but only a few systematic studies under the same conditions have been reported. Many effects of laser – beam interaction with a material surface are not well explained. Also, no comparison of features of plasma for materials of neighbouring elements is known.

Past investigations of magnesium plasma were performed in essentially different conditions. Usually, experiments were in vacuum with maximal power densities

[1]Corresponding author: Phone: +385 1 6129 670, +385 1 6129 607, Fax: +385 1 6129 605, E-mail: sanda.pleslic@fer.hr

several orders of magnitude larger than ours ((130 ± 25) MW/cm^2). They achieved higher ionisation stages, than our Mg I and Mg II [2].

Laser-induced aluminium plasma was investigasted in many experiments. Authors of Ref. [3] reported measurements with a N_2 laser, using 16 ns pulses, energy density of 1.3 J/cm^2, laser power 80 MW/cm^2, target in air and aluminium plasma scanned 0.1 – 0.4 mm above the target surface. From experimental data, they derived electron densities $(1 - 10)\ 10^{18}$/cm^3 and temperatures of about 1.5 eV. In another experiment [4], the same electron densities were obtained and electron temperatures were from 1.2 to 2 eV. Authors of experiment described in Ref. [5] were investigating aluminium plasma using Nd:YAG (DCR-4G) laser radiation at different wavelengths (266 nm, 355 nm, 532 nm) and using different radiation intensities (3, 7 and 10 10^{10} W/cm^2). They obtained electron temperatures from 0.8 to 4 eV. They also performed measurements at different distances from the target surface (up to 9 mm) and the target was in vacuum.

Similar experiments with silicon [6, 7] yielded values of electron temperature 1.4 – 1.6 eV and electron density of about 3.5 10^{18}/cm^3.

2. *Experimental set-up*

The experimental set-up used for time-integrated spectroscopic investigations of laser produced plasmas is shown in Fig. 1. The experiment was performed in air at atmospheric pressure. The N_2 laser produces (6 ± 1) ns pulses of 337.1 nm radiation with pulse energy of (11.0 ± 0.7) mJ. The laser was operated at the repetition rate of 0.2 Hz. The pulse shape (Fig. 2) was measured by a fast biplanar photodiode (FND 100A) coupled to a digital signal analyser (Tektronics DSA 602A).

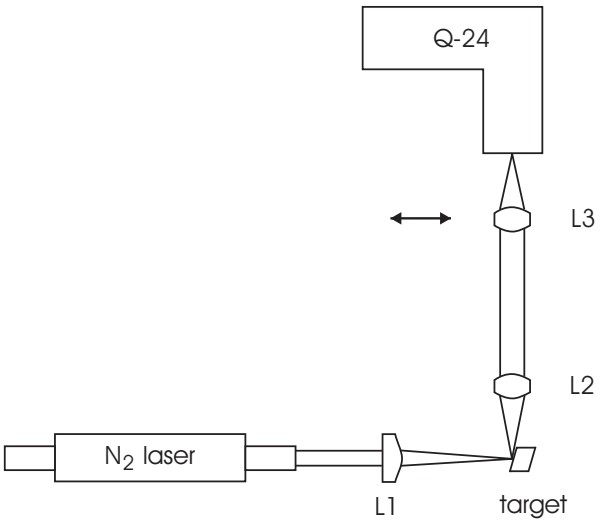

Fig. 1. Experimental set-up.

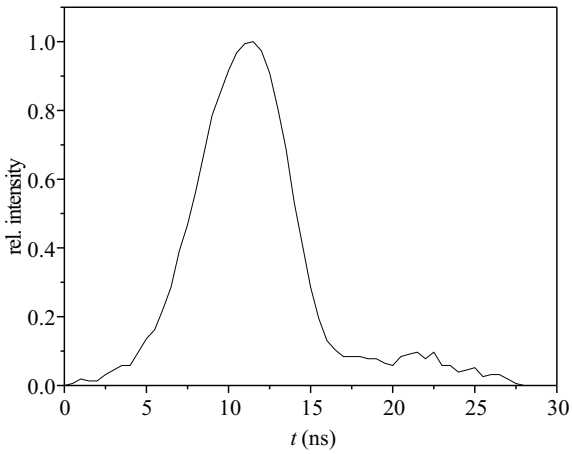

Fig. 2. Temporal profile of the N_2 *laser pulse. The FWHM of the pulse is 6* ns.

The N_2 laser radiation was focused onto a target by a 160 mm FL quartz lens. The target surface was almost perpendicular to the laser beam axis. Pure aluminium, silicon and magnesium were used as target materials. The laser beam was not uniform over the beam area, so the size and shape of the focal spot and the energy distribution on the target were measured separately. A quasi-3-dimensional plot of the energy distribution within the focal spot on the target is shown in Fig. 3. The size of the focal spot was measured to be about 0.4×3.4 mm. The plasma plume was imaged onto the entrance slit of a Carl Zeiss Q-24 single-prism quartz spectrograph, which is capable of covering the spectral range from 240 nm to 550 nm. Lenses used for this purpose were UV achromats (see Fig. 1). The plasma radiation was transformed into a parallel light beam by the lens L2 and

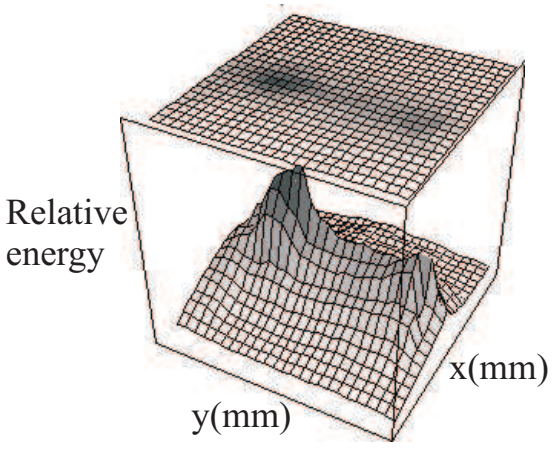

Fig. 3. A quasi-3-dimensional plot of energy distribution within the focal spot (area of 1.2×3.8 mm *is shown) on the target. The energy distribution is given in relative units.*

then focused onto the entrance slit of the spectrograph by the lens L3. The lens L3 was mounted on a stage which can be precisely translated, allowing the scanning of the plasma image across the entrance slit of the spectrograph in the direction perpendicular to the target surface (Fig. 4). Between 20 and 30 laser pulses were necessary to produce a satisfactory spectrum on the film. A calibrated tungsten filament lamp was employed as intensity standard and an iron spark as a standard for wavelength calibration.

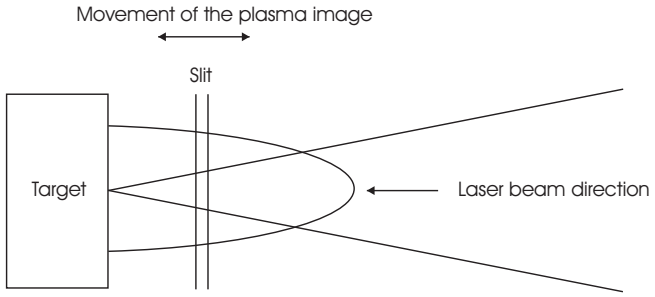

Fig. 4. The position of the spectrograph entrance slit relative to the target surface and direction of the laser beam.

3. Determination of electron density and temperature

The electron density was determined from the broadening of emission lines. The dominant broadening mechanism in laser-produced plasmas is Stark broadening [8]. Other broadening mechanisms can be neglected so that the electron density can be calculated from the measured FWHM of a Stark-broadened line

$$N_e = N_0 \frac{FWHM}{w_0} \tag{1}$$

where N_e is the electron density, *FWHM* is the measured full width at half-maximum of the considered line and w_0 is line *FWHM* given for a standard electron density N_0. Stark broadening parameters that we have used in our calculation are listed in Table 1. Electron temperatures were determined from the relative intensities of two spectral lines of successive ionisation stages. Successive ionisation stages were used because of the small difference in energy of the upper levels of spectral lines from the same ionisation stage resulting in large uncertainties in temperature calculated this way. Energy difference is increased by the ionisation energy of the lower ionisation stage.

$$\frac{I(1)}{I(2)} = \frac{A_{\mathrm{mn}}(1)}{A_{\mathrm{mn}}(2)} \, \frac{g_{\mathrm{m}}(1)}{g_{\mathrm{m}}(2)} \, \frac{\lambda_0(2)}{\lambda_0(1)} \sqrt{\left(\frac{kT}{\chi_H}\right)^3} \exp\left(-\frac{\Delta E}{kT}\right) \frac{1}{4\sqrt{\pi^3}\, a_0^3 N} \tag{2}$$

Here 1 refers to all data for the spectral line emitted by ions of the higher ionisation stage and 2 for the spectral line emitted by ions of the lower ionisation stage.

TABLE 1. Stark broadening parameters used for the determination of the electron density. All parameters are given assuming a reference electron density of $N_0 = 10^{18}/\mathrm{cm}^3$. *Stark broadening parameter,* w, *corresponds to the line FWHM and is given in* nm. *Ionic broadening parameter* α *is dimensionless. Data are taken from Ref. [8].*

Line	λ (nm)	T(K)	5000	10000	20000	40000	80000
Mg II	292.9	w	0.087	0.108	0.140	0.178	0.204
	293.7	α	0.130	0.111	0.089	0.076	0.066
Mg I	309.1	w	8.420	8.000	7.260	6.320	5.280
	309.6	α	0.604	0.629	0.677	0.749	0.857
Mg I	332.9	w	1.032	1.374	1.798	2.140	2.280
	333.6	α	0.253	0.202	0.168	0.145	0.139
Mg II	448.1	w	1.590	1.566	1.544	1.588	1.708
	448.1	α	0.164	0.164	0.168	0.164	0.155
Al I	256.8	w	0.698	0.896	1.094	1.216	1.232
	257.7	α	0.250	0.209	0.180	0.164	0.164
Al II	281.6	w	0.068	0.086	0.111	0.141	0.161
	281.6	α	0.120	0.104	0.085	0.070	0.063
Al I	308.2	w	0.576	0.562	0.528	0.486	0.436
	309.2	α	0.177	0.183	0.190	0.202	0.221
Al I	394.4	w	0.240	0.304	0.396	0.490	0.542
	396.1	α	0.145	0.123	0.101	0.085	0.079
Si I	243.9	w	0.071	0.089	0.115	0.145	0.163
	245.2	α	0.133	0.114	0.092	0.079	0.073
Si II	385.3	w	0.324	0.362	0.380	0.386	0.384
	386.2	α	0.104	0.098	0.095	0.092	0.092
Si I	390.5	w	0.179	0.226	0.292	0.366	0.412
	390.5	α	0.133	0.114	0.092	0.079	0.073
Si II	412.8	w	0.464	0.570	0.652	0.638	0.606
	413.0	α	0.133	0.144	0.104	0.104	0.108

$I(1)$ and $I(2)$ are relative line intensities, $A_{\mathrm{mn}}(i)$ are the corresponding transition probabilities, where m denotes the upper and n the lower level of the observed line, $g_{\mathrm{m}}(i)$ are the statistical weights of the upper levels, $\lambda_0(i)$ are the wavelengths of the line centres in vacuum, $E_m(i)$ are the energies of the upper line levels, kT is the thermal energy, χ_H is the ionisation energy of the hydrogen atom in vacuum (13.6 eV), a_0 is the Bohr atomic radius and N_e is the electron density. ΔE is the energy difference between the energy of the upper level of line 1 of the ion in the

higher ionisation state and the energy of the upper level of line 2 of the ion in the lower ionisation state, corrected for the ionisation energy in vacuum and due to the plasma interactions [8, 9]. Parameters of spectral lines used for the determination of electron density and temperature are tabulated in Table 2.

TABLE 2. Parameters of spectral lines used for the determination of electron density and temperature in plasma reported in this article [17, 18, 19]. λ_0 *is the wavelength of the line centre in vacuum,* g_m *is the statistical weight of the upper level,* E_m *is the energy of the upper level,* A_mn *is the transition probability.*

Line	Transition		λ_0 (nm)	g_m	E_m (eV)	A_mn (10^8 s^{-1})
Mg II	3p-4s	^{2}P^0-^{2}S	293.4	2	8.7	3.50
Mg I	3s3p-3s4d	^{3}P^0-^{3}D	309.5	15	6.7	0.56
Mg I	3s3p-3s5s	^{3}P^0-^{3}S	333,4	3	6.4	0.29
Mg II	3d-4f	^{2}D-^{2}F^0	448.1	14	11.6	2.23
Al I	3s^2(^{1}S)3p-3s^2(^{1}S)nd	^{2}P^0-^{2}D	257.5	6	4.8	0.26
Al II	3s3p-3s4s	^{1}P^0-^{1}S	281.6	3	11.8	3.83
Al I	3s^2(^{1}S)3p-3s^2(^{1}S)3d	^{2}P^0-^{2}D	308.9	10	4.0	0.74
Al II	3s^2(^{1}S)3p-3s^2(^{1}S)4s	^{2}P^0-^{2}S	395.6	2	3.1	1.47
Si II	3s3p^2-3s^2(^{1}S)4p	^{2}D-^{2}P^0	385.6	6	10.1	0.28
Si I	3s^{2}3p^2-3s^{2}3p4s	^{1}S-^{1}P^0	390.6	3	5.1	0.12
Si II	3s^2(^{1}S)3d-3s^2(^{1}S)4f	^{2}D-^{2}F^0	412.8	14	12.8	1.42

4. *Experimental results*

We observed features of the laser-produced plasmas from three neighbouring elements (magnesium, aluminium and silicon). In all measurements, laser parameters were kept the same to allow direct comparison of the results.

4.1. *Magnesium*

The estimated electron densities are around $10^{18}/\mathrm{cm}^3$ and electron temperatures about 1.7 eV (kT_e). The Debye shielding factor for this density and temperature is $r = 0.64$ which satisfies $r \leq 0.8$ and the condition (13.51) from Ref. [9] for the validity of the local thermodynamic equilibrium. The ionic broadening parameter α must be $\alpha \leq 0.5$ to satisfy the same condition. In this work, α was found to be between 0.1 and 0.3 for the investigated lines. Thus, the ionic contribution to line widths is small and can be disregarded, being only a few percent of the electronic line broadening. In such cases, the line width becomes a linear function of the electron density. For magnesium, we scanned the plasma image from the target surface and took data up to 0.60 mm above it in 0.05 mm steps. The electron

density and temperature as function of the distance from the magnesium target are shown in Fig. 5.

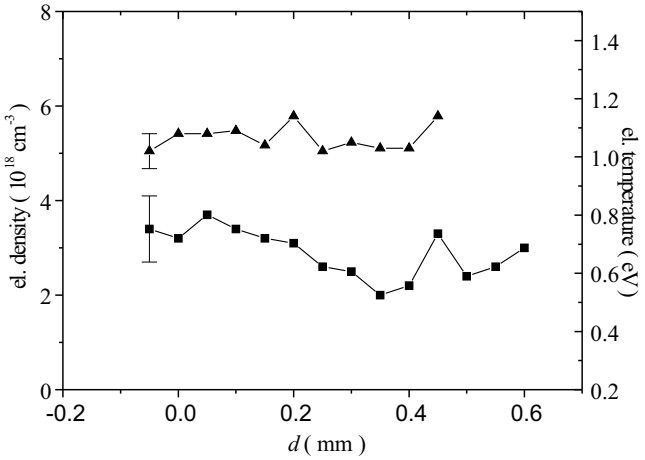

Fig. 5. The electron density (■) and temperature (●) as a function of the distance d from the target surface for magnesium.

4.2. Aluminium

The procedures for the calculations of the electron density and temperature for aluminium were the same as for magnesium. The ionic broadening parameter α was found to be between 0.1 and 0.2, so its effect on line widths can also be neglected.

Most data for aluminium were measured before [4], so we only made a control measurement to check the consistency of results at the distance of $d = 0.10$ mm from the target surface (Table 3). The results obtained are in agreement with those obtained before.

TABLE 3. The electron density N_e and the electron temperature T_e determined from observed aluminium spectral lines at the distance of $d = 0.10$ mm from the target surface. N_e^* and T_e^* are the averaged values.

Line	λ (nm)	N_e (10^{18}) cm^{-3}	T_e (eV)
Al I	394.4 396.2	2.1	1.7
Al I	308.2 309.3	1.5	1.7
Al II	281.6	6.0	1.5
Al I	257.5	0.8	1.1
		$N_e^* = 2.6 \pm 0.5$	$T_e^* = 1.5 \pm 0.4$

4.3. Silicon

The ionic broadening parameter α for silicon lines was even smaller, between 0.10 and 0.15 mm. The silicon plasma was scanned the same way as the magnesium plasma but from target surface to 0.30 mm above the surface (Fig. 6) because at larger distances plasma emission was too weak to be recorded.

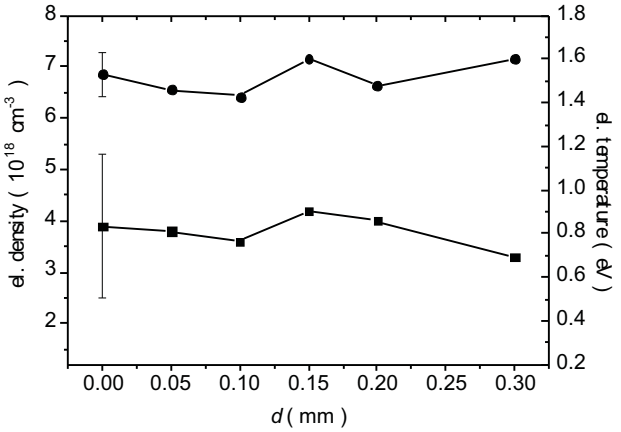

Fig. 6. The electron density (■) *and temperature* (●) *as a function of the distance d from the target for silicon.*

4.4. Other materials

It is interesting to note that all three target materials are metallic. Smaller trials with other metals (Cu, Ti, Fe, Zn, Pb) [10, 11] revealed that in general it is easy to generate plasmas from them. On the other hand, experiments with insulators (C, B, different plastics, glass) [12] failed to produce any detectable plasma at all. Only molecular spectra of corresponding molecules could be detected, with vibrational temperatures around 0.1 eV.

5. Discussion

Main parameters of the target materials used in the experiments are summarized in Table 4, while the determined plasma parameters are summarized in Table 5.

In addition to the experimentally determined electron density N_e^{exp} and electron temperature T_e^{exp}, we used a simple numerical model of target heating to model the target behaviour in our experiments. This model was initially developed in early 1990s [1] and includes temperature dependence of material constants (A, R, κ) describing material properties and experimentally observed laser pulse profile. In the meantime, the model was improved and expanded, so we could estimate different effects of target heating by changing initial parameters [13]. First, we modelled

TABLE 4. Main material parameters of the target materials. Z is the atom number, A is the absorption coefficient, R is the reflection coefficient and κ is the thermal conductivity coefficient. A, R and κ are given at room temperature.

Z	Target	Ground-state electron configuration	Ground level	Ionisation energy (eV)	A (nm^{-1})	R	κ (W/cmK)
12	Mg	$1s^2 2s^2 2p^6 3s^2$	$^1S_0$	7.6	0.07	0.69	1.59
13	Al	$1s^2 2s^2 2p^6 3s^2 3p$	$^2P^0_{1/2}$	6.0	0.15	0.94	2.37
14	Si	$1s^2 2s^2 2p^6 3s^2 3p^2$	$^3P_0$	8.2	0.11	0.56	1.31

TABLE 5. Plasma parameters determined from experiment in comparison with theoretically determined parameters. $N_e^{\rm exp}$ and $T_e^{\rm exp}$ are average electron density and temperature calculated from experimental data. Tmodel is the surface layer temperature calculated from numerical modelling. $T^{\rm effus}$ is the surface layer temperature calculated from effusion model.

Target	$N_e^{\rm exp}$ (10^{18} cm^{-3})	$T_e^{\rm exp}$ (eV)	$T^{\rm model}$ (eV)	$T^{\rm effus}$ (eV)
Mg	2.9 ± 0.8	1.1 ± 0.1	5.8	3.9
Al	2.6 ± 0.5	1.5 ± 0.4	5.4	3.6
Si	3.5 ± 2.0	1.5 ± 0.1	5.9	4.0

TABLE 6. Maximal temperatures of target surface (in eV*) with laser pulse energy density as parameter.*

Target material	Energy density (J/cm^2)		
	0.8	1.0	1.2
Mg	5.31	5.76	6.10
Al	4.90	5.50	5.91
Si	5.62	5.95	6.23

heating of different targets by changing the value of the energy density. In Table 6 maximal derived temperatures reached during the target surface heating are given.

The dependence of maximal temperature on energy density is weak because losses due to plasma radiation, which at temperatures above 1 eV dominate, increase with the fourth power of temperature according to the Stefan-Boltzmann law [14]. $T^{\rm effus}$ is the temperature in plasma immediately above the target surface,

determined from the effusion model in which material transition in vapour phase and gas kinetics in the so called Knudsen layer decrease maximal temperature to approximately 2/3 of the surface temperature [1, 15, 16]. In numerical modelling of target heating, the real laser pulse profile with duration of 6 ns (*FWHM*) and energy density 1.0 J/cm^2 was used. After the beginning of the pulse, target surface transits from one phase to another (solid, liquid, vapour) very quickly. Only 7 – 8 ns after the beginning of the pulse, the surface is vaporized and maximal temperature between 5 and 6 eV is reached in the next few ns (Fig. 7). The analysis of these results shows that plasma is near its maximal temperature ($T \geq 0.9\ T_{\max}$) for only 5 ns, and around 1 eV for much longer (45 ns). This explains the apparent difference between the calculated maximal temperatures and the observed average electron temperatures.

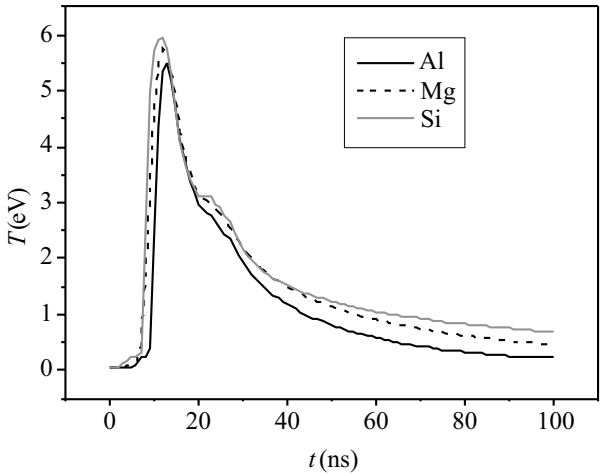

Fig. 7. Target heating for Mg, Al and Si *with laser pulse energy density 1.0* J/cm^2.

6. Conclusion

Experimental investigations of laser-produced plasmas of three materials (magnesium, aluminium, silicon) are described in this work. We used time-integrated spectroscopy of the plasma radiation. The plasma was produced by nanosecond (6 ns) nitrogen laser pulses with wavelength of 337.1 nm, focussed perpendicularly onto the target surface. The energy distribution of the laser radiation in the focal region of the focusing lens had maximal power density of about 130 MW/cm^2 with the maximal energy density of about 1.1 J/cm^2. After the beginning of the laser pulse, material rapidly transits from one phase to another (solid, liquid, vapour). The vapour is almost instantaneously ionised and the maximal temperature of several eV is reached in the next few ns.

The measurements yielded electron densities of about 10^{18}/cm^3 and electron temperatures of about 1.5 eV. These values do not match maximal values directly.

They are averaged over time and we cannot relate them with conditions at target surface. So, we tried to estimate maximal temperatures of target surface layers using numerical modelling. These values are 4 – 5 times higher than electron temperatures determined experimentally. After the heating to very high temperature, plasma expands rapidly, but this expansion is slowed down and finally stopped by the resistance of the surrounding atmosphere (air at normal pressure in our experiment). The modelling also shows that plasma at temperatures around 1 eV lasts much longer than at near maximal temperature, thus explaining the experimentally determined lower temperatures in the range of 1 – 1.5 eV.

The most intense plasma radiation was observed at a distance of about 0.10 mm above the target surface. The plasma development can be followed to about 0.60 mm for Mg and Al and to 0.30 mm for Si. At larger distances, plasma emission became undetectable. During plasma expansion, electron temperatures remained almost constant and electron densities showed a tendency to weakly decrease.

Significant changes of features of laser-produced plasmas of materials of the neighbouring elements was not found. We showed that optical depth of a particular material is the main parameter for plasma production. Transparent materials have very a large optical depth, so the energy is absorbed in thicker layers and in our experimental conditions plasma would not be produced. Working at a frequency lower than the plasma frequency, metals have very high R and small optical depth and surface layer heating is much stronger. All three target materials (Mg, Al, Si) have small optical depth of the order of about 10 nm and produced plasmas were at temperatures of several eV.

References

[1] Ž. Andreić, *Spectroscopic Investigations of Aluminium Plasma Produced by a Nitrogen Laser*, Ph. D. Thesis, Zagreb (1993).

[2] G. A. Vergunova et al., Physica Scripta **55** (1997) 483.

[3] Ž. Andreić, V. Henč-Bartolić and H.-J. Kunze, Physica Scripta **48** (1993) 331.

[4] Ž. Andreić, V. Henč-Bartolić and H.-J. Kunze, Physica Scripta **47** (1993) 405.

[5] R. Tambay, R. Singh and R. K. Thareja, J. Appl. Phys. **72** (1992) 1197.

[6] V. Henč-Bartolić, Ž. Andreić, D. Gracin, H.-J. Kunze and M. Stubičar, Fizika A (Zagreb) **6** (1997) 97.

[7] Ž. Andreić, V. Henč-Bartolić, D. Gracin and M. Stubičar, Appl. Surf. Sci. **136** (1998) 73.

[8] H. R. Griem, *Plasma Spectroscopy*, McGraw-Hill Book Company, New York (1964).

[9] G. Bekefi, *Principles of Laser Plasmas*, John Wiley and Sons, New York (1976).

[10] V. Henč-Bartolić, Ž. Andreić, D. Gracin, H.-J. Kunze and M. Stubičar, Fizika A (Zagreb) **4** (1995) 449.

[11] V. Henč-Bartolić, Ž. Andreić, M. Stubičar and M., H.-J. Kunze, Fizika A (Zagreb) **7** (1998) 205.

[12] T. Atwee, L. Aschke and H.-J. Kunze, J. Phys. D: Appl. Phys. **33** (2000) 2263.

[13] S. Pleslić and Ž. Andreić, Vacuum **72** (2004) 439.

[14] E. N. Sobol, *Phase Transformations and Ablation in Laser-Treated Solids*, John Wiley and Sons, New York, 1995).

[15] B. Braven, K. G. Casey and R. Kelly, Nucl. Instr. Meth. Phys. Res. B **58** (1991) 463.

[16] R. Kelly, J. Chem. Phys. **92** (1990) 5047.

[17] W. C. Martin and R. Zalubas, J. Phys. Chem. Ref. Data **9** (1980) 1.

[18] W. C. Martin and R. Zalubas, J. Phys. Chem. Ref. Data **8** (1979) 817.

[19] W. C. Martin and R. Zalubas, J. Phys. Chem. Ref. Data **12** (1983) 323.

LASEROM PROIZVEDENA PLAZMA NA POVRŠINAMA Mg, Al AND Si

U ovom se radu opisuje eksperimentalno istraživanje laserski proizvedenih plazmi Mg, Al i Si. Plazme se proizvode nanosekundnim (6 ns) impulsima dušikovog lasera (337,1 nm) s maksimalnom energijskom gustoćom od 1,1 J/cm^2 i spektroskopski proučavaju u ultraljubičastom i vidljivom području. Eksperiment daje elektronske gustoće reda veličine 10^{18}/cm^3 i elektronske temperature oko 1,5 eV u proizvedenim plazmama. Numeričko modeliranje zagrijavanja mete daje 4 – 5 puta više temperature od onih koje su eksperimentalno određene. Nismo našli značajniju promjenu svojstava laserski proizvedenih plazmi za navedena tri susjedna elementa. Pokazali smo da je optička dubina pojedinog materijala glavni parametar u proizvodnji plazme.